Advanced Steel Construction – Vol. 22 No. 2 (2026) 237–243
DOI:10.18057/IJASC.2026.22.2.9

EXPERIMENTAL STUDY ON MECHANICAL PROPERTIES OF PREFABRICATED BEAM AND SLAB UNITS OF NEW ASSEMBLED RAFT FOUNDATION

Ji-Zhi Su [1], Chen-Lei Wang [2], Wen-Tao Qiao [2, 3, *], Wu-Chen Zhang [1] and Li-Huan Wang [1]

[1] *Economic and Technological Research Institute, State Grid Hebei Electric Power Co., Ltd, Shijiazhuang, China*
[2] *School of Civil Engineering, Shijiazhuang Tiedao University, Shijiazhuang, China*
[3] *Key Laboratory of Roads and Railway Engineering Safety Control (Shijiazhuang Tiedao University), Ministry of Education, Shijiazhuang, China*
** (Corresponding author: E-mail: qwt@stdu.edu.cn)*

ABSTRACT

Prefabricated foundations offer numerous advantages such as convenient construction, high bearing capacity, energy efficiency, environmental friendliness, and less wet work on-site. Accordingly, this study introduces a novel structural system based on an assembled beam-slab foundation. To further explore the mechanical properties of the precast beam slab units in the modular beam-slab foundation, experimental research and numerical simulation were conducted. Test findings indicate that the structure primarily undergoes bending-type failure. From the yielding of the specimen to the attainment of the ultimate load, the specimen undergoes significant displacement changes, indicating that the structure possesses good bending resistance and ductility. Based on the experimental results, an accurate finite element model was established for parametric analysis. The findings indicate that the bearing capacity of the foundation slab is significantly influenced by parameters such as reinforcement ratio and slab thickness, with the reinforcement ratio having the most pronounced effect. The ultimate load-carrying capacity increases with the reinforcement ratio, composite slab thickness, and concrete strength. In contrast, the thickness of the C-section steel has the least effect on the bearing capacity, with the foundation slab's bearing capacity remaining virtually unchanged.

ARTICLE HISTORY

Received: 19 January 2025
Revised: 23 July 2025
Accepted: 2 August 2025

KEYWORDS

Assembled raft foundation;
Prefabricated beam and slab units;
Static loading test;
Numerical simulation

1. Introduction

With rapid urbanization, the number of high-rise buildings in China has been steadily increasing, leading to greater loads transferred from superstructures to foundations. When the superstructure is subjected to heavy loads and the foundation exhibits limited bearing capacity, conventional independent or strip foundations often fail to satisfy deformation control requirements. Under such circumstances, raft foundations have been widely applied. Raft foundations not only meet the requirements of different foundation bearing capacities but also make more effective use of underground space, thus having broad application prospects and promotional value[1, 2].

At present, numerous scholars have conducted extensive experimental research and theoretical analysis on raft foundations. Among them, Wang[3] conducted experimental studies on single-span and multi-span beam-slab raft foundations with different slab thicknesses, revealing the distribution pattern of foundation reaction under various load conditions. Yu et al.[4]conducted full-scale experimental studies on two groups of beam-slab raft foundation specimens. During the loading process, the foundation exhibited overall positive bending, while the internal slab grid areas showed characteristics of negative bending. Akash et al.[5] investigated the influence of factors such as pile length, number of piles, and diameter on the load distribution of pile-raft foundations. Xi et al.[6] carried out experimental research on the load-bearing behavior of pile-raft foundations, and the study demonstrated that pile-raft slab foundations outperform conventional pipe pile foundations. Hoang et al.[7] investigated the long-term performance of three pile-raft foundations with different numbers of piles, revealing that load magnitude significantly impacts the distribution of loads between the raft and piles over time. Anuj et al.[8] conducted an analysis on pile-raft foundations revealing that their bearing capacity is considerably higher than raft foundations, with pile length, spacing, and soil density showing strong positive correlations with load-bearing performance. Overall, these studies highlight the structural advantages and performance improvements of raft and pile-raft foundations under various loading and soil conditions, but there remains a need for further exploration of more efficient structural forms tailored for prefabrication and assembly.

With the development of prefabricated buildings, the feasibility of adopting reasonable prefabricated foundation forms has attracted increasing attention. Several scholars have conducted in-depth research on this topic. Rasmussen[9] proposed a prefabricated strip foundation made of EPS, which is only suitable for small buildings with no more than two floors. Adams[10] introduced a prefabricated concrete block foundation component that connects to the superstructure by arranging rebar and casting concrete on-site. Dae Hong Kim et al.[11] designed a micropile foundation for transmission towers, where each foundation component is connected by bolts. Catalano[12] proposed a detachable prefabricated foundation component suitable for temporary buildings with relatively small upper loads, where the foundation components are bolted to the foundation beams. Li et al.[13] proposed a novel prefabricated foundation structure for transmission lines and conducted numerical simulation analysis. The results indicate that the structure satisfactorily fulfills the functional demands. In summary, current prefabricated foundations are mostly used in structures with small upper loads, and related research is relatively limited. Therefore, studying a prefabricated foundation structure with better bearing capacity and a wider range of applications is of great significance.

In recent years, a large number of scholars have carried out comprehensive research on composite slabs. Ranzi et al.[14] conducted experiments to evaluate the flexural performance of composite slabs with steel strand, proposing a theoretical calculation model suitable for prestressed composite slabs. Crisinel et al.[15] introduced an analytical approach for calculating the load-bearing capacity of composite slabs. Qiao et al.[16] proposed a novel cold-formed thin-walled steel-concrete composite slab and conducted experimental studies on its flexural performance, the test results revealed that this structure exhibits good mechanical performance. Vainiūnas et al.[17] investigated the shear performance of profiled steel sheet-concrete composite slabs and developed a calculation method for their horizontal cross-sectional strength. Mistakidis et al.[18] conducted experimental studies on the flexural performance of embossed steel-concrete composite slabs, with results indicating that the embossing on the steel significantly improves the flexural performance of the slabs. Rios et al.[19] proposed a computational approach to analyze the shear bond behavior in steel-concrete composite slabs. Zhang et al.[20] carried out experimental research on a novel thin-walled steel-wood composite panel, demonstrating its excellent bending performance. Xiang et al.[21] proposed a calculation method for the vertical shear resistance of ribbed steel-concrete composite slabs.

It can be observed that current research on composite slabs primarily focuses on unidirectional composite slabs, with relatively few studies on bidirectional composite slabs. Additionally, the application of composite slabs in foundation structures is also relatively limited. In response to this situation, this paper proposes a prefabricated beam-slab foundation structural system, composed of multiple standardized prefabricated beam-slab units. This structure has advantages in easy construction, energy saving, material saving, and high bearing capacity. The mechanical performance between prefabricated beam-slab units in prefabricated foundations directly influences the overall behavior of the structure. Therefore, this paper focuses on certain prefabricated beam-slab units within the prefabricated beam-slab foundation. Through static load tests, the mechanical performance of the foundation bottom slab and the slab connectors was investigated, revealing the failure characteristics and load-bearing mechanisms of the specimens under vertical loads. Additionally, numerical simulation analysis utilizing the experimental data was conducted to validate the correctness of the finite element model. Based on the experimental and finite element verification, a parametric analysis was performed to explore

the impact of factors such as concrete strength, reinforcement ratio, composite slab thickness, and C-shaped steel thickness on the static performance of the foundation base slab.

2. The structure system

The new prefabricated beam-slab foundation system presented in this paper is depicted in Fig. 1. The structure mainly consists of foundation beams, foundation bottom plates, and various connection nodes. In the prefabricated raft foundation, the foundation slab primarily bears the bending moment. Considering the span requirements for the raft foundation, the foundation slab adopts grooved slab, which consists of prefabricated beam-slab units with ribbed edges, as shown in Fig. 1(b). This structure is grooved along the thickness direction of the slab, not only reducing material usage but also effectively lightening the weight of the structure. Meanwhile, the surrounding ribbed beams significantly enhance the global stiffness and load-bearing capacity of the structure. The prefabricated beam-slab units are composed of C-shaped steel, reinforcement, and concrete. The C-shaped steel is placed in the ribbed beam section of the prefabricated beam-slab unit. The internal reinforcement is connected to the surrounding C-shaped steel by welding, while bolt holes are pre-formed in the web section to enable linkage with inter-panel connectors. The connectors between the prefabricated beam-slab units consist of inner and outer sleeves, with the inner and outer sleeves locking together to join the prefabricated beam-slab units.

The structure of the foundation beams and their connection nodes is shown in Fig. 1(c). When designing the structure, it was considered that the large cross-section of the profile steel and its good continuity could effectively disperse and transfer loads, providing better local shear and punching shear resistance. Therefore, T-shaped steel is embedded in the foundation beams, with a single layer of reinforcement arranged at the top. In the process of making the precast foundation beam, the concrete is not poured at the joint, and the exposed profile steel and reinforcement are used for the node connections. When designing the connection nodes between the foundation beams, the node is divided into upper, middle, and lower parts, as shown in Fig. 1(c). This connection node consists of three steel tubes of different sizes: the upper square steel tube has slots for fixing the rebar inside the composite beam, the middle square steel tube has bolt holes in the extended end plate, which connect to the web of the extended T-shaped steel of the composite beam via bolts, and the lower square steel tube has an upward opening to support the flange of the extended T-shaped steel of the composite beam.

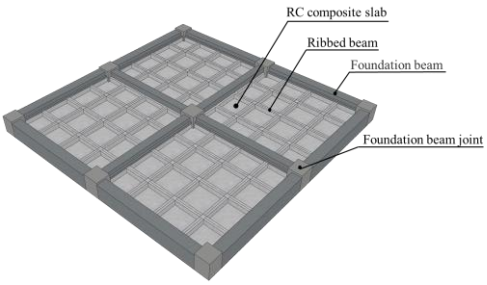

(a) assembled raft foundation

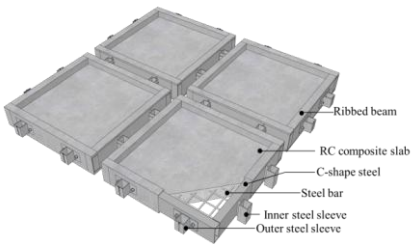

(b) prefabricated beam and slab units

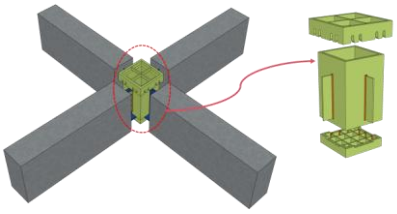

(c) foundation beam joint

Fig. 1 structural diagram of assembled raft foundation

3. Experiment investigation

3.1. Specimen details

To study the mechanical performance of the prefabricated beam and slab units and its connectors in this structure, a full-scale foundation slab specimen was fabricated. The specimen consists of four prefabricated beam-slab units and four prefabricated foundation beams, as shown in Fig. 2 Each prefabricated beam-slab unit includes steel-reinforced concrete slab and ribbed beams. The reinforced concrete (RC) composite slab is 200 mm thick, and the ribbed beam section dimensions are 100×300 mm. Inside the RC composite slab, a single layer of rebar with a diameter of 12 mm is arranged, with a spacing of 100 mm. The concrete used for the specimen is C30, and the rebar is HRB400 grade steel. The C-shaped steel is Q235 grade, with dimensions of 250×80×9 mm. The connectors between the slabs are prefabricated square steel tubes, available in two models: 110×110×5 mm and 100×100×6 mm. The composite beam dimensions are 400×500 mm, with internal T-shaped steel made of Q235 grade steel, model dimensions of 250×200×10×16 mm. All bolts used in the specimen are grade 8.8 high-strength bolts, with a diameter of M20 and a hole diameter of d_0=22 mm. The detailed dimensions of the prefabricated beam-slab units are shown in Fig. 3.

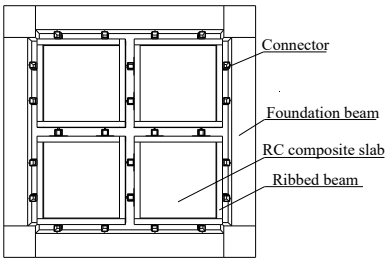

Fig. 2 Installation completion diagram

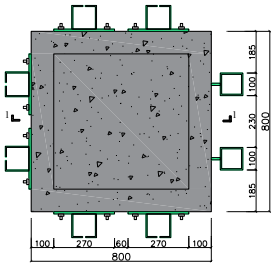

(a) Plan drawing

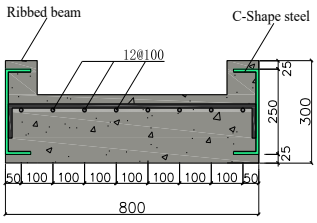

(b) 1-1 cross-section drawing

Fig. 3 Detail of prefabricated beam and slab units (mm)

3.2. Material properties

In accordance with GB/T 228.1-2010[22] and GB/T 2975-2018[23], tensile tests were employed to characterize the mechanical properties of the experimental steel. Three specimens each were taken from the C-shape steel and T-shape steel used in the experiment, and tensile tests were performed on a universal testing machine. The mechanical characteristics of the tested steel are shown in Table 1. The prefabricated beam-slab units used reinforcement with a diameter of 12 mm. To measure the mechanical properties of this reinforcement, three 500 mm long samples were selected for tensile tests. The mechanical properties of the tested reinforcement are shown in Table 2.

C30 grade concrete served as the material for all test specimens. To measure the compressive performance of concrete, three sets of 150 × 150 ×

150 mm concrete cubes were reserved when pouring the concrete for the specimens. Compressive strength tests were conducted on these reserved concrete cubes according to the Chinese standard GB/T 50081-2002[24]. The measured material properties of the concrete are listed in Table 3.

Table 1
Material property of section steel

Specimen number	Yield strength /MPa	Ultimate strength /MPa	Elastic modulus /10^5 MPa	Elongation /%
T-1	306.0	390.1	2.02	32.1
T-2	302.3	394.2	2.07	33.5
T-3	310.2	390.7	2.04	35.1
Average	306.2	391.7	2.04	33.5
C-1	305.5	390.3	2.03	30.1
C-2	302.5	392.3	2.02	30.6
C-3	309.5	396.2	2.04	30.2
Average	301.6	394.3	2.07	30.3

Note: T-1 is the steel specimen for the slab connector, and C-1 is the steel specimen for the web of the C-shaped steel.

Table 2
Material property of rebar

Specimen number	Rebar diameter /mm	Yield load /kN	Yield strength /MPa	Maximum tension /kN	Ultimate strength /MPa
G-1	12	46.52	411.3	69.25	612.3
G-2	12	46.78	413.6	69.94	618.3
G-2	12	47.46	419.6	69.59	615.2
Average	12	46.92	414.8	69.59	615.3

Table 3
Material property of concrete

Concrete grade	Axial compressive strength /MPa	Average /MPa	Elastic modulus /104 MPa	Average /10^4 MPa
C30	32.7	32.1	3.16	3.12
	30.2		3.08	
	33.5		3.12	

3.3. Testing program

3.3.1. Loading protocol

The experiment used a 1000-ton multifunctional testing machine to apply vertical loads. In order to simulate the loads experienced by the specimen during actual service conditions, the specimen was inverted during installation, with the bottom of the base plate facing upward for load application. During loading, a secondary distribution beam was used to achieve four-point loading, with the load points located at the center of the prefabricated beam-slab units. The specimen is a two-way slab, and the support system consists of four steel beams and four steel columns. When installing the specimen, it was placed on the steel frame, with the steel beams supporting the bottom of the composite beam. This support configuration restricted vertical displacement while allowing rotation along all four slab edges, and is therefore classified as a simply supported boundary condition. The loading setup is shown in Fig. 4.

3.3.2. Loading steps

Displacement-controlled loading was applied during the test. Prior to the formal loading process, a preload of 10 kN was applied to the specimen and maintained for 5 minutes to ensure the proper functioning of all systems and to eliminate any gaps between the specimen and the support system. The displacement-controlled loading in the formal testing stage was performed at 3 mm/min, with a 3-minute hold at each increment. This loading rate was selected with reference to the Chinese standard GB/T 50152-2012[25], which recommends a loading speed within the range of 0.5–5 mm/min for quasi-static testing. During the test, the specimen was monitored using force sensors, and its deformation under different loading stages was carefully observed.

Fig. 4 Example of a figure

3.3.3. Layout of measuring points

During the loading process, the deflection change, crack development, inter-plate connector strain and steel bar strain of the specimen were mainly observed. Fig. 5 illustrates the layout of the displacement and strain gauges. A total of four displacement gauges were used in the experiment. Gauge W1 was placed at the center of the specimen, gauges W2 and W3 were placed at the 1/4 points of the specimen's centerline, and gauge W4 was placed at the center of the composite beam to observe changes in specimen deflection. Strain gauges were distributed on the slab connectors, rebar, and C-shaped steel.

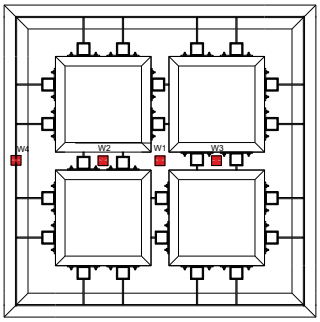

(a) Layout of Displacement meter

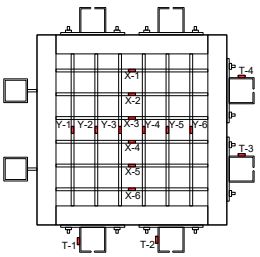

(b) Layout of Strain gauges

Fig. 5 Layout of measurement points

4. Failure process

During the early loading stage, the specimen remained in the elastic range without significant deformation. A progressive increase in deflection was observed as the applied load increased. At approximately 35% of the peak load, fine cracks appeared at the center of the bottom of the specimen along the diagonal direction, but there was no noticeable flexural deformation. With the gradual increase of applied load, crack propagation was observed at the specimen's central region, accompanied by the initiation of 45° diagonal cracks at the mid-span of the bottom surface of the RC composite slab. When the load reached 51% of the peak load, minor cracking appeared in the concrete at the ribbed beam node connection area, and the number of cracks at the RC composite slab increased. As the load increased to 62% of the peak, slight sounds were heard from within the specimen, indicating it had reached the yield state, with a mid-span deflection of 6.72 mm, and more cracks appeared at the RC composite slab. At peak load, the crack width at the RC composite slab increased, more cracks appeared in the ribbed beam node connection area, and the rebar inside the RC composite slab had yielded. As shown in Fig. 6, at the end of the test, large cracks developed in the tensile zone of the concrete, and

the maximum deflection reached 18 mm, approximately 1/160 of the structure's span, which is considered as the failure criterion of the structure.

(a) The cracks of ribbed beam

(b) The cracks of composite slab

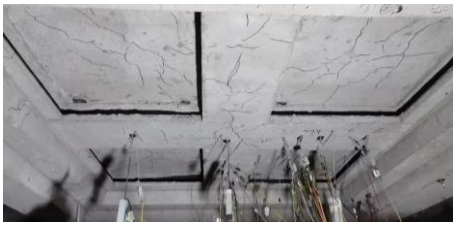

(c) The cracks of the whole structure

Fig. 6 The failure of structure

5. Analysis of test results

5.1. Bearing capacity and ductility

As shown in Fig. 7, the load-displacement curve can be segmented into three phases, with the specimen exhibiting elastic behavior during the initial loading at low loads. The curve exhibits a nearly linear relationship, indicating good synergy between the section steel, rebar, and concrete within the prefabricated beam-slab unit. As loading progresses, cracks begin to develop in the tensile zone of the concrete, and the curve enters the elastoplastic phase. Due to the cracking of the concrete, the section steel and rebar inside the RC composite slab bear the load and also provide some constraint on the development of concrete cracks. With the progressive growth in both the quantity and width of cracks, the synergy between the section steel, rebar, and concrete weakens. The rate of load increase diminishes while the rate of displacement increase becomes more pronounced. When the load reaches its peak, the curve enters the failure stage. At this point, the rebar within the specimen yields, the deformation of the specimen increases, and the load gradually decreases until the specimen is destroyed and the test ends.

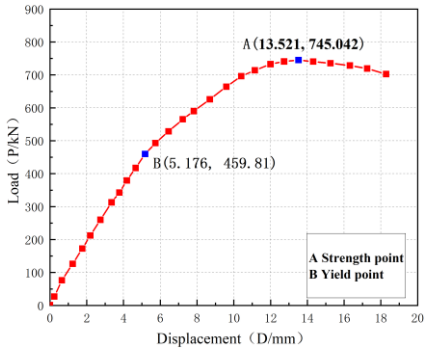

Fig. 7 Load-displacement curves

An essential metric for evaluating structural deformation capacity is the ductility coefficient of the component. The test results are illustrated in Table 4, indicating that the ductility coefficient of this specimen is 3.53, which demonstrates that the structure has good ductility.

Table 4
Ductility coefficient of the specimens

Specimen number	Δ_y / mm	*Ny* /kN	Δ_u / mm	*Nu* /kN	DI
Specimen 1	5.176	459.81	18.29	757.19	3.53

Note： Δ_y is the yield displacement， Δ_u is the ultimate displacement，*Ny* is the yield strength，Nu is the ultimate strength，DI is the ductility coefficient

5.2. The analysis of concrete deflection variation

In order to better observe the deflection variation of the two-way slab specimen, displacement gauges were installed at the specimen's mid-span, quarter-span, and support regions. The deflection variation at the centerline of the specimen during the test was monitored, as illustrated in Fig. 8. The curve exhibits an approximately sinusoidal pattern. When the load is less than $0.6N_u$, the specimen remains in the elastic phase, with deflection increasing linearly and at a relatively slow rate. When the load exceeds $0.6N_u$, the specimen transitions into the elastic-plastic phase, and the rate of deflection change accelerates. Additionally, the general pattern of the curve demonstrates that the mid-span undergoes a more pronounced change in deflection compared to the quarter-span regions.

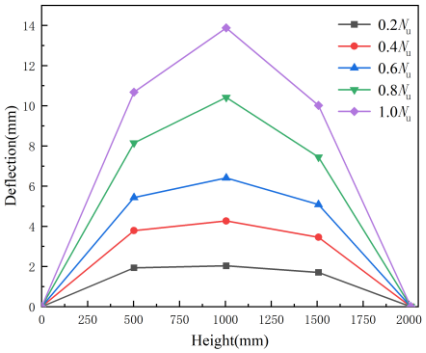

Fig. 8 Deflection curve of concrete

5.3. Strain analysis of rebar

Fig. 9 presents the strain distributions of the reinforcement along the X and Y directions within the composite slab. It can be observed that under vertical loading, the rebars are all in a tensile state. The strain patterns of the reinforcement in both X and Y directions exhibit similar behavior: strain increases more rapidly as the location approaches the mid-span. In the initial loading phase, the specimen is in the elastic phase, and the strain growth of the rebars is slow. As the load increases, the concrete begins to crack, and the rebars bear more load, leading to a rapid increase in strain until the specimen fails.

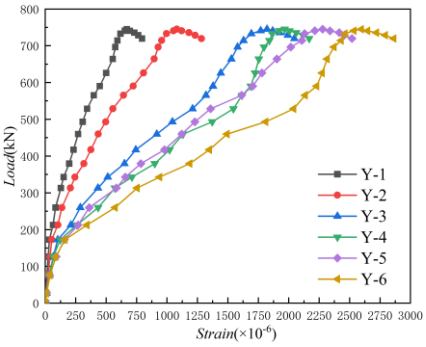

(a) Reinforcement strain of Y-direction

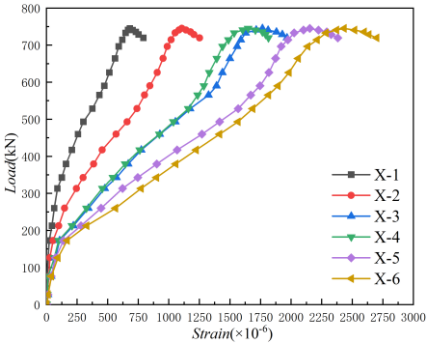

(b) Reinforcement strain of X-direction

Fig. 9 Load-strain curve of reinforcement

5.4. Strain analysis of connector

The load-strain curves of the inter-slab connectors reflect the stress and deformation characteristics of the connection nodes under vertical loads. The load-strain curves of the node connectors obtained from the experiment are illustrated in Fig. 10. It can be observed that the strain values of the curves are all positive, indicating that all the connectors are in a tensile state. The strain development trends of the connectors in different regions are essentially consistent. In the initial loading phase, the curves display linear growth. As loading progresses, concrete cracks develop continuously, and the strain of the connectors gradually increases. According to the material property test data, the yield strain of the connectors is 1.5×10^3. It can be seen that connectors have not reached yield stress. At the ultimate load stage, the T-4 connector at mid-span exhibits the highest tensile strain, aligning well with the experimental findings.

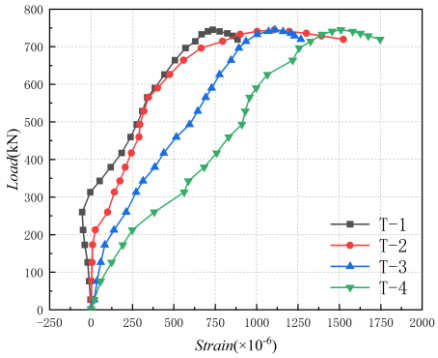

Fig. 10 Load-strain curve of connectors

6. Finite element modeling investigation

6.1. Finite element model

6.1.1. General

To analyze the mechanical characteristics of the prefabricated beam-slab units in the novel foundation system, finite element modeling (FEM) was performed in ABAQUS. The model dimensions were consistent with the experimental specimens. Both concrete and internal section steel were modeled using C3D8R elements, while the reinforcement was simulated using 3D two-node truss elements. The material constitutive relationships were based on material property tests: concrete elements utilized a plastic damage model with a concrete strength grade of C30 and an elastic modulus of E=31200 MPa; the section steel and reinforcing bars were simplified into bilinear models based on relevant test data. During the mesh generation process, a sensitivity analysis was performed by simulating models with different mesh sizes to determine the optimal mesh size for each material element. The final mesh sizes were 50 mm for concrete elements, 35 mm for section steel, and 15 mm for reinforcing bar truss elements. An illustration of the FEM is provided in Fig. 11.

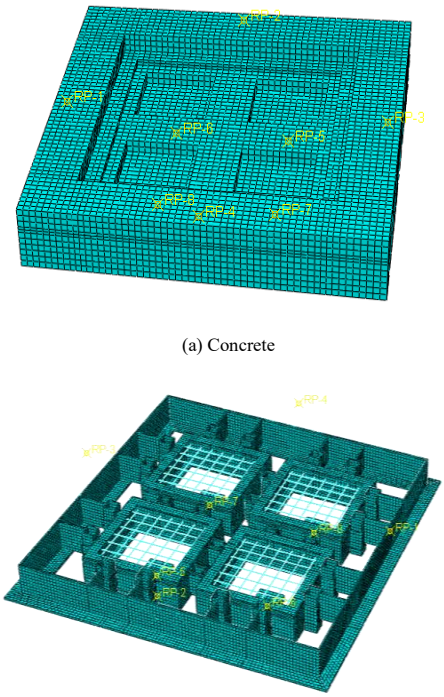

(a) Concrete

(b) Steel frame

Fig. 11 Finite element model

6.1.2. Interactions

Surface-to-surface contact constraints were employed to simulate the interaction between the connectors and the section steel. The normal contact was modeled as hard contact, while tangential behavior adhered to Coulomb friction with a coefficient of 0.15. The rebars and the C-shaped section steel were constrained using TIE constraints, with the Embedded method employed to embed the steel framework formed by the C-shaped steel and the rebars into the concrete. Additionally, steel pads were placed at the loading points of the model. The pads were tied to the model, ensuring that they remained tightly connected throughout the loading process without any relative sliding.

6.1.3. Boundary conditions

The FEM uses identical boundary conditions and loading procedures as those applied in the experiment. In applying boundary conditions, only the translational degrees of freedom along U1, U2, and U3 are restricted, whereas the rotational degrees of freedom around the X, Y, and Z axes remain free. Four-point loading is employed during the loading process. Four rigid pads are placed at the loading points, which are bonded to the model. The loading surface is coupled at one point, and the loading is applied using displacement control.

6.2. Numerical simulation results and analysis

6.2.1. Comparison of failure modes

The cracking condition of the specimen can be clearly seen through the tensile damage of the concrete. As illustrated in Fig. 12, the FEM failure modes align well with the experimental observations. Cracking primarily occurs in the composite slab region and the central part of the ribbed beams. The cracks within the composite slab are symmetrically arranged under vertical loads. The crack distribution in the FEM closely matches the experimental results.

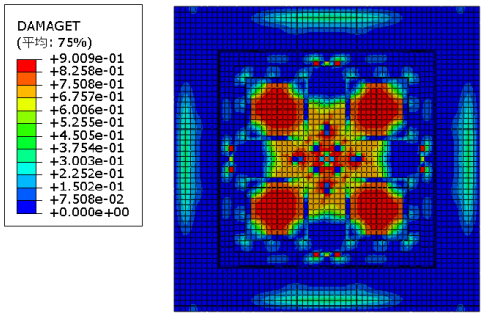

(a) Tensile damage of FEM

(b) Cracks and failure in test

Fig. 12 Comparison of damage characteristics

6.2.2. Comparison of load-displacement curves

The load-displacement curves from both the FEM analysis and the experimental tests are compared in Fig. 13. The finite element simulation results closely match the experimental data, particularly in the elastic range where discrepancies are negligible. However, as the curve enters the elastoplastic stage, the simulation results exhibit some discrepancy compared to the experimental findings. Compared to experimental data, the FEM slightly overestimated the load capacity, which can be attributed to the simplified model's exclusion of concrete–steel bond-slip interactions. Overall, the error between the two results is within 15%. The consistency between the experimental and FEM curves indicates that the simulation results are reliable.

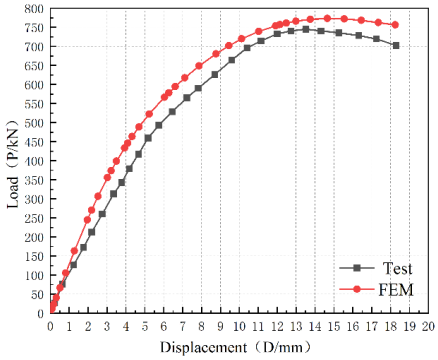

Fig. 13 Comparison of FEM and tested Load-Displacement curves

7. Parameter analysis

The effects of different parameters on the load-bearing behavior and failure characteristics of foundation slab units are investigated through parametric analysis, based on the established and validated FEM. In conjunction with the load-bearing characteristics and capacity variation patterns of the test specimens, four key influencing factors, namely concrete strength, rebar diameter, composite slab thickness, and C-shaped steel thickness, were selected as the focus of the research.

7.1. Concrete strength

Based on the commonly used concrete strength grades in current engineering practice, the concrete strength in the FEM models was set sequentially as C20, C30, C40, and C50. Load-displacement responses obtained from FEM simulations for concrete grades C20 through C50 are illustrated in Fig. 14. The results indicate increases in flexural capacity of 11.58%, 8.04%, and 6.11% as the grade progresses from C20 to C30, C30 to C40, and C40 to C50, respectively. Under different concrete strength grades, the specimens exhibited distinct elastoplastic behavior. As the concrete strength grade increased, the specimens exhibited a notable improvement in bending load capacity, indicating that concrete strength is a key factor affecting the static behavior of prefabricated beam-slab units. Moreover, as the concrete strength increased, the failure mode tended to become more brittle, and the plastic deformation capacity was slightly reduced. Additionally, the contribution of concrete strength to further enhancement of bearing capacity became progressively less significant. Therefore, in practical applications, a suitable concrete grade can be selected based on engineering requirements and economic considerations.

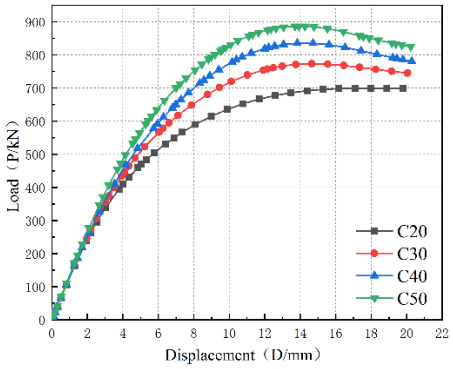

Fig. 14 Load displacement curve of different concrete strength

7.2. Reinforcement ratio

According to the requirements for reinforcement ratio in GB 50010-2010, the reinforcement diameters in the model were set sequentially as 10 mm, 12 mm, 14 mm, and 16 mm. Specimens with various reinforcement ratios in the composite slab exhibit distinct load-displacement curves, as shown in Fig. 15. It can be observed that as the reinforcement ratio in the slab increases from 0.44% (corresponding to a rebar diameter of 10 mm) to 1.06% (corresponding to a rebar diameter of 16 mm), the bending load-bearing capacity increases by 50.5%. The ultimate load-bearing capacity corresponding to adjacent rebar diameters differs by 12.7%, 16.1%, and 15.2%, respectively. This indicates that the bending load-bearing capacity of the foundation slab is strongly affected by the reinforcement ratio in the composite slab. With an increase in reinforcement ratio, the tensile capacity contributed by the reinforcement is improved, resulting in a significant enhancement of the foundation slab's bending load-bearing capacity. Additionally, the increment in load-bearing capacity between successive reinforcement ratios diminishes as the reinforcement ratio increases, indicating a trend of diminishing returns within a certain range. Therefore, considering structural design codes and experimental findings, a rebar diameter ranging from 10 mm to 14 mm is recommended for the composite slab.

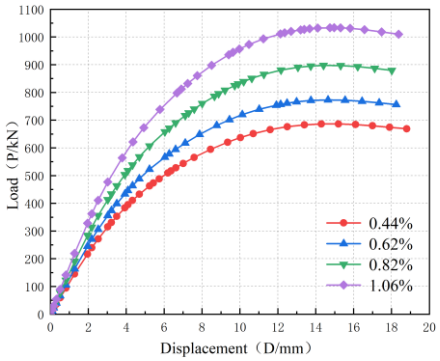

Fig. 15 Load displacement curve of different reinforcement ratio

7.3. Thickness of composite slab

This section focuses on the influence of composite slab thickness on the mechanical performance of prefabricated beam-slab units. To this end, when establishing the FEM, only the thickness of the composite slab was varied while the height of the rib beam remained constant. As shown in Fig. 16, the FEM results indicated a 16.3% increase in ultimate load-bearing capacity when the slab thickness was raised from 200 mm to 220 mm, followed by an additional 16.1% increase as it reached 240 mm. The findings indicate that changes in slab thickness substantially impact the structural capacity of the foundation base slab. Additionally, from the figure, it can be seen that as the slab thickness increases, the mid-span displacement at the peak load also gradually increases, suggesting that within a certain range, increasing the slab thickness helps improve the overall structural ductility, allowing the foundation base slab to withstand larger deformations.

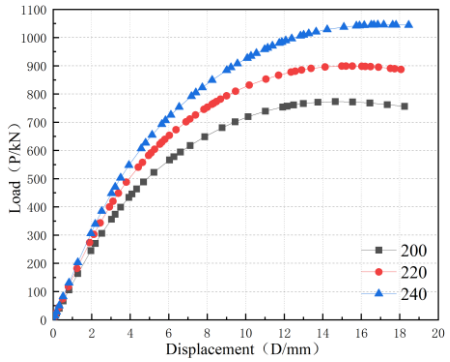

Fig. 16 Load displacement curve of different slab thickness

7.4. Thickness of C-shaped steel

C-shaped steel is an important component of the steel framework in prefabricated beam-slab units. This part investigates the influence of C-shaped steel thickness on bending capacity by varying its thickness while maintaining all other variables constant. The FEM assigns C-shaped steel thicknesses of 5 mm, 7 mm, 9 mm, and 12 mm sequentially. and finite element numerical simulations are conducted. As illustrated in Fig. 17, the load-displacement behavior of the foundation base slab is depicted. It can be observed that as the thickness increases from 5 mm to 12 mm, the ultimate load-bearing capacity of the foundation base slab shows a slight increase. Specifically, the bending load-bearing capacity increases by 4.6% when the C-shaped steel thickness is raised from 5 mm to 12 mm. It can be concluded that variations in the thickness of the C-shaped steel have limited effect on the load-bearing capacity of the foundation slab. During structural design, smaller dimensions of C-shaped steel may be considered, providing a reference for optimizing both the economy and performance of the section steel.

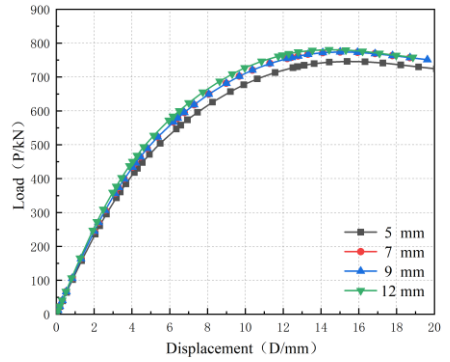

Fig. 17 Load displacement curve of different C-Section Steel thickness

8. Conclusions

This paper conducted an experimental study on the mechanical performance of foundation slabs and inter-slab connectors under vertical loads in prefabricated beam-slab foundations. The study analyzed the failure characteristics, bearing capacity, ductility, and strain patterns of reinforcement and connectors of the test specimens under static load tests. Additionally, a numerical simulation analysis of the test specimens was conducted using the finite element software ABAQUS. The conclusions drawn are as follows:

(1) Under vertical loading, the specimen exhibited overall bending failure characteristics. During failure, multiple cracks appeared in the tensile zone of the composite slab concrete, while no significant damage was observed in the node core area. This satisfies the design principle of "strong node, weak component," indicating that the structure possesses good bending load-bearing capacity.

(2) The load-displacement curve showed distinct elastic, elastoplastic, and failure stages. The curve experienced significant displacement changes from the specimen's yield point to the ultimate load, indicating good ductility performance of the structure.

(3) The failure characteristics of the FEM are in good agreement with the experimental results. The load-displacement curve obtained from the numerical simulation matches closely with the experimental curve, indicating that the FEM effectively simulates the real behavior of the test specimen. Thus, the FEM is reliable.

(4) A parametric analysis was conducted considering four influencing factors: concrete strength, reinforcement ratio, composite slab thickness, and C-shaped steel thickness. The results indicate that the bending load-bearing capacity of the foundation base plate is positively correlated with concrete strength, reinforcement ratio, and composite slab thickness, with reinforcement ratio having the most significant impact on load-bearing capacity. Conversely, the thickness of the C-shaped steel has negligible influence on the bending capacity of the foundation base plate.

Acknowledgments

This research was supported by Natural Science Foundation of Hebei Province for Distinguished Young Scholars (Grant No. E2022210084).

References

[1] Weidong Kang, Huang Bei, Gu Hao. Application of Raft Foundation in Transmission Line Engineering[J]. Academic Journal of Engineering and Technology Science,2020,3.0(8.0): 61-69.
[2] Teng L, Yamin W, Linjie C, et al. Research on design of the prefabricated foundation in substations[J]. Journal of Physics: Conference Series,2021,1904(1): 1-20.
[3] Shuguang W. Experimental study on failure behavior of beam-slab raft foundation under uniform column load [J]. Journal of Civil Engineering, 2006, (10): 97-101.
[4] Yu D, Gong J, Jiang S, etc. Experimental study on reaction deformation and failure characteristics of beam-slab raft foundation under column under uniform and non-uniform loads [J]. Building Science, 2015,31 (05): 29-35.
[5] Priyadarshee A, Kumar V, Sharma K, et al. Study on the load sharing in piled raft foundation[J]. Multiscale and Multidisciplinary Modeling, Experiments and Design,2024,7(3):3005-3015.
[6] Xi X, Wentao G, Tatsunori M, et al. Bearing characteristics of model piled raft foundations supported by sheet piles[J]. International Journal of Physical Modelling in Geotechnics,2023,24(1):38-53.
[7] Hoang T L, Xiong X, Matsumoto T. Effect of pile arrangement on long-term settlement and load distribution in piled raft foundation models supported by jacked-in piles in saturated clay[J]. Soils and Foundations,2024,64(2):101426-.
[8] Anuj C, Sandip V. Experimental investigation of inclined compressive loading on a piled raft foundation[J]. Ocean Engineering,2023,287(P1):1-9.
[9] Rasmussen T V Ø. Integrated Strip Foundation Systems for Small Residential Buildings[J]. The Open Construction & Building Technology Journal, 2010, 4: 39-53.
[10] Adams F H. Concrete footer block and foundation system formed therefrom[P]. U.S. Patent 4903450,1989-5-2.
[11] Kim, D. H., Pyo, W. S., Kim, J. G., et al. Base body of electric transmission tower using micropile[P]. U.S. Patent 20170191239A1,2017-7-6.
[12] Catalano S F R. Precast foundation assembly for mobile homes[P]. U.S. Patent 3879905,1975-4-29.
[13] Guanhua L, Rui L, Xu D, et al. Design of prefabricated foundation for 66kV tower assembly and simulation of mechanical properties and grounding current density distribution[J]. Journal of Physics: Conference Series,2022,2296(1): 1-6.
[14] Ranzi G, Ostinelli A. Ultimate behaviour and design of post-tensioned composite slabs[J]. Engineering Structures,2017,150: 711-718.
[15] Crisinel M, Marimon F. A new simplified method for the design of composite slabs[J]. Journal of Constructional Steel Research,2004,60(3):481-491.
[16] Qiao W, Yan X, Zhu R, et al. Flexural properties of new cold-formed thin-walled steel and concrete composite slabs[J]. Journal of Building Engineering,2020,31:1-13.
[17] Vainiūnas P, Valivonis J, Marčiukaitis G, et al. Analysis of longitudinal shear behaviour for composite steel and concrete slabs[J]. Journal of Constructional Steel Research,2006,62(12):1264-1269.
[18] Mistakidis S E, Dimitriadis G K. Bending resistance of composite slabs made with thin-walled steel sheeting with indentations or embossments[J]. Thin-Walled structures,2008,46(2):192-206.
[19] Ríos, J. D, Cifuentes, H, Concha, A. M.-D. L, et al. Numerical modelling of the shear-bond behaviour of composite slabs in four and six-point bending tests[J]. Engineering Structures, 2017,133:91-104.
[20] Zhang A, Chen Z, Liu J. Flexural performance of innovative thin-walled steel–timber composite floor slabs[J]. Engineering Structures,2024,318:118676-118676.
[21] Da X, Yuqing L, Yichi S, et al. Vertical shear capacity of steel-concrete composite deck slabs with steel ribs[J]. Engineering Structures,2022,262:114396.
[22] Metallic Materials - Tensile Testing - Part 1: Method of Test at Room Temperature GB/T 228.1-2010 [S]. Beijing: Standards Press of China, 2010.
[23] Steel and Steel Products - Location and Preparation of Test Pieces for Mechanical Testing GB/T 2975-2018 [S]. Beijing: Standards Press of China, 2018.
[24]Standard for Test Methods of Mechanical Properties of Concrete GB 50081-2002 [S]. Beijing: China Architecture & Building Press, 2002.
[25] Standard Test Methods for Concrete Structures GB/T 50152-2012 [S]. Beijing: China Architecture & Building Press, 2016.